

PanoLAM: Large Avatar Model for Gaussian Full-Head Synthesis from One-shot Unposed Image

Peng Li^{1*†} Yisheng He^{2*‡} Yingdong Hu^{1†} Yuan Dong² Weihao Yuan² Yuan Liu¹
 Zilong Dong² Yike Guo¹

¹HKUST ² Tongyi Lab, Alibaba Group



Figure 1. PanoLAM creates high-fidelity Gaussian full-heads with one-shot unposed images in a single forward pass in seconds.

Abstract

We present a feed-forward framework for Gaussian full-head synthesis from a single unposed image. Unlike previous work that relies on time-consuming GAN inversion and test-time optimization, our framework can reconstruct the Gaussian full-head model given a single unposed image in a single forward pass. This enables fast reconstruction and rendering during inference. To mitigate the lack of large-scale 3D head assets, we propose a large-scale synthetic dataset from trained 3D GANs and train our framework using only synthetic data. For efficient high-fidelity generation, we introduce a coarse-to-fine Gaussian head generation pipeline, where sparse points from the

FLAME model interact with the image features by transformer blocks for feature extraction and coarse shape reconstruction, which are then densified for high-fidelity reconstruction. To fully leverage the prior knowledge residing in pretrained 3D GANs for effective reconstruction, we propose a dual-branch framework that effectively aggregates the structured spherical triplane feature and unstructured point-based features for more effective Gaussian head reconstruction. Experimental results show the effectiveness of our framework towards existing work.

1. Introduction

Reconstructing head avatars from a single image is an important area of research within computer graphics and computer vision. The capability to generate high-fidelity head

*Equal Contribution † Work done during an internship with Alibaba Tongyi Lab. ‡ Corresponding Author

avatars opens up new possibilities in areas such as 3D telepresence, video conferencing, filmmaking, gaming, and augmented/virtual reality (AR/VR). However, efficiently creating digital head avatars that are high-fidelity and efficient in rendering is challenging, and various studies have tried to resolve this problem.

One line of work uses 3D Generative Adversarial Networks (3D-GANs) [2, 11] for the unconditional generation of 3D head avatars, which learn 3D generation models from 2D images paired with camera poses. Unlike 2D-GANs [33] for single-view generation, these approaches can generate face images with control over viewing angles. The pioneering work EG3D [11] introduces a triplane representation in Cartesian space to enable novel view synthesis after generation. The following works [2, 43] allow a wider range of viewing angles from the generated NeRF space and make 360° images synthesis possible. However, these GAN-based frameworks require time- and computation-consuming GAN-inversion [42] or test-time optimization [65] for image-conditioned generation during inference. Furthermore, the accurate camera pose of the input image is required for joint optimization of these inversion approaches. Rodin [77] and its follow-up [86] instead utilize diffusion models to generate triplanes of the head avatars. However, the multi-step diffusion process during inference still requires minutes of optimization for each case. Moreover, the costly ray marching hinders the rendering resolution of these NeRF-based frameworks. Though 2D super-resolution upsampling is proposed to improve the rendering efficiency and quality, it compromises 3D consistency.

In this work, we propose a feed-forward framework to generate a full-head Gaussian avatar given a single *unposed* image. This enables fast reconstruction and rendering of a 3D avatar during inference. However, this task presents certain challenges. **1)** The first hurdle lies in the lack of large-scale 3D head datasets for network training. To tackle this problem, we propose to leverage the prior knowledge in trained 3D GANs and sample a large-scale, diverse dataset from EG3D [11] and SphereHead [43]. We label and remove invalid cases manually to improve the quality of the dataset. **2)** The second challenge involves how to efficiently and effectively reconstruct the high-fidelity Gaussian head from a single unposed image. To overcome this, we propose two main designs for our framework. **i)** Firstly, to improve the network efficiency, we propose a coarse-to-fine reconstruction mechanism for high-fidelity Gaussian full-head reconstruction. Specifically, sparse points extract rich image features, craft the coarse shape, and are then upsampled for high-fidelity dense Gaussian head reconstruction. By leveraging the topology prior in the FLAME model, we also introduce an efficient network-free upsampling mechanism for features and point clouds densification. **ii)** Secondly,

to improve the effectiveness of the reconstruction process, we propose a dual-branch framework that hybridizes the unstructured point features and the structured spherical triplane features for the reconstruction of a Gaussian head. To distill the spherical triplane knowledge from the pretrained 3D GAN, we analyze its original feature aggregation manner and propose an efficient mechanism to effectively aggregate multi-layer features from the spherical triplane.

The principal contributions of our work can be summarized as follows:

- We propose PanoLAM, a large avatar model for *Gaussian full-head* reconstruction from *a single unposed* image.
- We propose a coarse-to-fine reconstruction mechanism for efficient and high-fidelity Gaussian full-head reconstruction. Built upon the topology prior in the FLAME model, we introduce an efficient network-free upsampling mechanism for points and features densification.
- We propose a dual-branch framework that hybridizes the representation of point and the spherical triplane prior from 3D GAN. An efficient aggregation mechanism is also proposed to effectively extract multi-layer features from the triplane.
- We propose a large-scale, diverse synthesis dataset for 3D avatar reconstruction and generation. To our knowledge, ours is the largest and most diverse 3D head avatar dataset.

2. Related work

3D Head Modeling Models. Various 3D representations have been applied for 3D head modeling, including mesh, Neural Radiance Fields (NeRFs) [54], Signed Distance Functions (SDFs), and Gaussian Splatting [35]. For mesh-based modeling, significant research [7, 45, 61] has been dedicated to representing 3D human heads with parametric textured meshes. However, predefined topologies constrain the capture of finer details and accessories such as hair and glasses, resulting in images that may appear unrealistic. More recent works [36, 48] try to improve the topology by deforming the FLAME model to cover these detailed areas. With the advent of NeRF for novel view synthesis, some recent works [3–5, 25–27, 31, 37, 46, 52, 59, 60, 73, 83, 89, 90, 95] also utilize NeRF for 3D head modeling and enable more realistic rendering. Along with NeRF, SDF, another implicit representation is also introduced into the 3D head modeling field [9, 85, 91, 92] to improve geometry quality, where each 3D position is assigned with the signed distance to the nearest surface. To enable more efficient rendering, the point-based [93] and Gaussian Splatting-based [14, 23, 51, 63, 66, 80] frameworks are also proposed. Although getting good performance, these 3D head modeling frameworks usually require minutes to hours of optimization from videos or multiview images with estimated camera pose for each person before usage, limiting

their capability of scaling up and applications that require fast reconstruction. Instead, our work introduces a framework that can generate a Gaussian *full-head* avatar from *a single unposed image in a single forward pass* within *seconds*.

3D Avatar Generative Models. One line of generative models utilizes 3D-aware Generative Adversarial Networks (GANs) [11] to synthesize view-consistent images by capturing the scene’s inherent 3D geometry and appearance from collections of training 2D images. Early approaches [24, 49, 55, 56, 68, 71] employ explicit 3D representations like meshes and voxel grids, while more recent studies [2, 11] utilize implicit representations for better image quality. EG3D [11] introduces a 3D triplane representation with GAN to generate heads that are capable of novel view synthesis. The following works [2, 43], further enable 360° novel-view synthesis. However, these GAN-based methods are mainly designed for unconditional generation, and require time- and computation-consuming techniques like GAN inversion [12, 42, 69] and test-time optimization [65] for image-conditioned generation. The slow optimization procedure during inference and the sacrifice in multi-view consistency hinder their real-world application. [6, 13, 74, 84] distill an encoding network from EG3D for efficient image-to-triplane generation, but can only generate views near the front face. Instead of using GAN-based frameworks, more recent works [77, 86] utilize diffusion models to generate triplanes of head avatars. However, the multi-step diffusion process is still slow and computation-consuming during inference. Several works [1, 17, 22, 41, 47, 70] also introduce generalizable animatable avatar generation, but cannot reconstruct full heads. Moreover, due to the slow rendering speed of NeRF, these triplane NeRF-based approaches usually render low-resolution images from NeRF and apply super-resolution networks to enhance image detail, leading to view inconsistencies. To enhance rendering speed and rendered image quality, recent works [16, 30, 40, 72] also utilize Gaussian Splatting [35] as the 3D representation for generation. Specifically, LAM [30] introduces a feedforward framework for single-shot animatable Gaussian head generation that can be animated and rendered in real-time on various platforms. However, it requires estimation of FLAME parameters for reconstruction, which is time-consuming, and the generated head can only be rendered from limited viewing angles due to the limited viewing angles in the training 2D videos. This work, instead, can reconstruct the 3D *Gaussian full-head* given a single *unposed image in a single forward pass* efficiently, thanks to our large-scale 3D training datasets and our coarse-to-fine and dual-branch network design.

3D Avatar Datasets. The quantity and quality of 3D training datasets are crucial to the capability and general-

Table 1. Comparisons of different 3D avatar datasets. * denotes 3D head with rough captured 3D hair shape.

Dataset	Sub.	Range	Hair	Dataset	Sub.	Range	Hair
BU-3DFE	100	front	✗	HeadSpace	1519	270°	✗
BU-4DFE	101	front	✓	FaceScape	938	360°	✗
BJUT-3D	500	front	✗	AVA-256	256	360°	✓
Bosphorus	105	front	✗	FaceVerse*	128	360°	✓
FaceWarhouse	150	front	✓	RenderMe360*	500	360°	✓
4DFAB	180	front	✗	SynHead100	100	360°	✓
BP4D-S	41	front	✓	Ours-Front	48,135	72°	✓
Nersemble	222	front	✓	Ours-360	117,186	360°	✓

izability of learning-based models. Various datasets have been introduced into this field in the past decades. However, as shown in Table 1, many datasets [10, 15, 18, 19, 32, 39, 67, 81, 87, 88] only capture the front region of the faces. Networks trained on these datasets cannot model the side and back region of the head well. Although recent works [29, 53, 58, 76, 94] introduce 360° datasets into this field, the number of subjects in these datasets is limited, hindering the generalizability of trained networks. Under the observation that it’s much easier for humans to remove bad cases from generated 3D avatars compared to directly modeling them, we utilize pretrained 3D-aware GANs to develop and label a large-scale 3D head dataset. Leveraging two prior models, EG3D for 72° front views and Sphere-Head for 360° view synthesis, our total dataset, after removing bad cases manually to improve the quality, consists of 5M images of 165K subjects. To our knowledge, ours is the largest and most diverse dataset for 3D Avatar generation.

3. Methodology

3.1. Overview

As shown in Fig. 2, given an unposed reference image, our framework generates the Gaussian full-head in an efficient coarse-to-fine and joint point-triplane manner, where dense point cloud and point features are densified from sparse ones and fused with the spherical triplane features for dense Gaussian head regression. As shown in the upper part of Fig. 2, in the coarse stage of the point branch, sparse vertices from the FLAME vertices interact with the extracted multi-level image features by stacked cross-attention modules for feature extraction and coarse Gaussian point reconstruction. The dense reconstruction stage leverages barycentric weights from FLAME subdivision to densify the coarse Gaussian point position and features for dense Gaussian points regression. To fully leverage the prior knowledge residing in the spherical triplane of 3D GAN, as shown in the bottom branch of Fig. 2, a spherical triplane branch is also introduced, and an efficient aggregation mechanism is proposed to aggregate the structured fea-

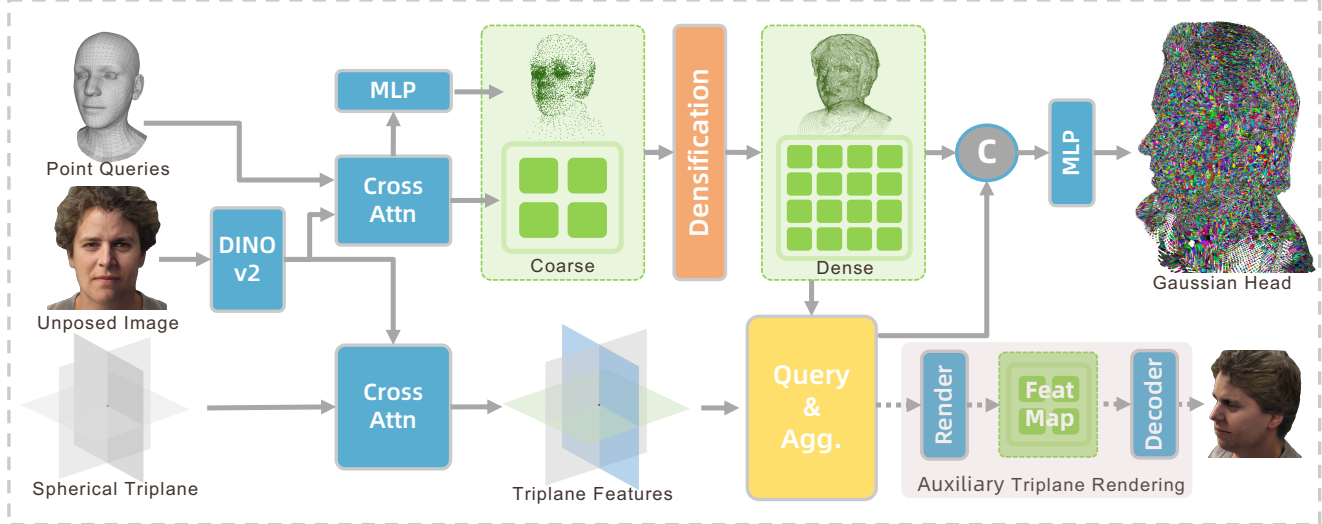


Figure 2. Overall Framework. Given an unposed head image as input, PanoLAM involves two branches to achieve single-pass 3D Gaussian head reconstruction: a point-based transformer for coarse-to-fine point shape reconstruction and point features extraction, and a spherical triplane transformer to distill prior knowledge from the pretrained 3D GAN. The unstructured point features and the queried and aggregated structured spherical triplane features are concatenated for high-fidelity Gaussian head regression. We add auxiliary triplane rendering in the triplane-branch for supervision during training.

tures from the spherical triplane using the densified point cloud, which are then concatenated with the unstructured point features for high-fidelity Gaussian head reconstruction.

3.2. Coarse-to-fine Gaussian Head Avatar Generation

The number of Gaussian points is one key factor that can affect the fidelity of the reconstructed Gaussian head, especially for the head avatar that contains sharp details like hair strands, mustaches, and wrinkles. The total number of Gaussian points should be large enough to produce these details. However, the large number of Gaussian points is hard to optimize during training, especially in our feed-forward pipeline, where the iterative densification operation in the traditional 3D Gaussian Splatting training pipeline is not applicable. To resolve this problem, unlike previous work [30] that directly regresses the dense point cloud, we introduce a coarse-to-fine mechanism. Specifically, sparse Gaussian points are first reconstructed for coarse shape reconstruction and then densified to dense Gaussians for high-fidelity details crafting. There are two advantages in the proposed design. Firstly, the sparse number of points enables efficient cross-attention with the image features for textures and shape features extraction, saving large computation and memory costs compared with a large number of points. Secondly, the sparse point can be well supervised and optimized for large deformation to carve the shape of the head, especially in regions that require large deformation from the original FLAME model, e.g., long hairs. Dense Gaus-

sian points upsampled from these correctly deformed sparse points can focus more on texture details crafting, which are much easier to optimize.

Coarse Gaussian Head Generation To fully leverage the head shape prior that resides in the FLAME model, we initialize the coarse Gaussian point with sparse vertices (about 5000 points) on the neutral FLAME model in the canonical space. Our target is to regress the deformation offset for shape refinement of regions that FLAME cannot model, e.g., long hairs, glasses, and caps. To supervise the shape deformation with RGB input images, Gaussian attributes for each point are also regressed for differentiable Gaussian Splatting.

To get started, we assign positional embedding to each point and utilize learnable multi-layer perceptron (MLP) modules to project the channel of features into the token channel C_t of transformers as follows:

$$F_{P_0} = \text{MLP}(\gamma(V)), \quad (1)$$

where V is the spatial position of each vertex and γ the L-frequency sinusoidal encoding as in NeRF [54]. To extract the texture and shape information in the given unposed image, we utilize the pre-trained DinoV2 [57] for feature extraction. Inspired by [30, 64], we fuse features derived from both shallow and deep layers to obtain both local and global image features F_I . Specifically, an MLP fuses the $\{5, 12, 18, 24\}$ layers of features in DinoV2 into C_t token

channels of features as:

$$F_I = \text{MLP}(\mathcal{C}(F_{D_5}, F_{D_{12}}, F_{D_{18}}, F_{D_{24}})), \quad (2)$$

where F_{D_i} is the i th layer of DinoV2 features and \mathcal{C} is the concatenation operation.

Given mapped point features F_P and extracted image features F_I , we utilize L_A layers of stacked cross-attention modules $\mathcal{A} = \{\mathcal{A}_i\}_{i=1}^{L_A}$ from Transformer [75] for feature extraction from image to point cloud as follows:

$$F_{P_i} = \mathcal{A}_i(F_{P_{i-1}}, F_I), \quad (3)$$

where F_{P_i} is the i th layers of point features in the stacked cross-attention layers.

Following the feature extraction process, each point retains its distinct features. Using these features, we develop decoding headers \mathcal{D} , composed of multilayer perceptrons (MLPs), to predict the deformation offset $O_k \in \mathbb{R}^3$ to refine the individual’s detailed shape. Gaussian attributes for each point are also regressed for rendering, including color $c_k \in \mathbb{R}^3$, opacity $o_k \in \mathbb{R}$, scale factors $s_k \in \mathbb{R}^3$, and rotation $R_k \in SO(3)$. This decoding process is as follows:

$$\{c_k, o_k, s_k, R_k, O_k\}_{k=1}^{M_C} = \mathcal{D}(F_{P_k}), \quad (4)$$

where $M_C = 5023$ represents the total number of Gaussians in the coarse reconstruction stage, and F_{P_k} denotes the extracted point feature for point P_k . Although predicting deformation offsets for each point can enhance the shape, freely moving these points may also negatively impact reconstruction results. We therefore restrict the range of deformation offset to be within $[-\epsilon_{O_C}, \epsilon_{O_C}]$.

Efficient Point Cloud Densification After the reconstruction of the coarse Gaussian head, we obtain a sparse point cloud that describes the shape of the target head avatar in the image, each point is also attached with rich features extracted from the image. We then densify these points and features for high-fidelity dense Gaussian head reconstruction. Unlike previous methods [44, 82] that require a network trained to upsample sparse points, we leverage the topology in the FLAME mesh and propose an efficient densification strategy that utilizes the barycentric weights from mesh subdivision to densify the point cloud and feature. Our key observation is that after the deformation in the coarse reconstruction stage, the topology between each point mostly remains as the original FLAME vertices. Thereafter, we can precompute the barycentric weights for point cloud densification utilizing mesh subdivision on FLAME. Specifically, given the original FLAME model, we perform subdivision for faces that are larger than a threshold λ_{area} , the position of newly added vertices v' can be computed from the three vertices of the original face

with barycentric weights as:

$$v' = \sum_{i=1}^3 (w_i \cdot v_i), \quad (5)$$

where w_i and v_i are the barycentric weight and vertex coordinate of the original face, respectively. After the deformation in the coarse reconstruction stage, each vertex moves to a new position w.r.t the predicted offset as $p_i = v_i + O_i$. Then new added point p' with its attached point features p'_F can be interpolated with barycentric weights as:

$$p' = \sum_{i=1}^3 (w_i \cdot p_i), \quad (6)$$

$$p'_F = \sum_{i=1}^3 (w_i \cdot p_{F_i}), \quad (7)$$

where p_{F_i} is the extracted features from the last cross-attention blocks in Equ. (9). In this way, we can efficiently densify the point and point features.

Dense Gaussian Head Generation. After getting the dense point position with dense point features, we can utilize them for dense Gaussian head regression. Rather than using only unstructured point features for prediction, we also aggregate features from the structured spherical triplane for more effective Gaussian attributes regression, which we will discuss in the next section. Denote F_{P_i} the i th point feature and F_{T_i} the aggregated spherical triplane feature for point P_i , the dense Gaussian head attributes and a small deformation residual can be regressed similarly to the coarse one as:

$$\{c_i, o_i, s_i, R_i, O_i\}_{i=1}^{M_D} = \mathcal{D}(\mathcal{C}(F_{P_i}, F_{T_i})), \quad (8)$$

where \mathcal{C} denotes the concatenation operation, M_D the number of dense Gaussian points, and O_i the deformation residual restricted within $[-\epsilon_{O_D}, \epsilon_{O_D}]$.

3.3. Spherical Triplane Prior Knowledge Distillation

In the previous section, we obtain the dense point cloud with its attached point features extracted from the unposed image. Inspired by TriplaneGaussian [96], where structured triplane features are efficiently sampled by the unstructured point cloud for better Gaussian attributes regression, we introduce a spherical triplane branch to distill the knowledge from the trained SphereHead [43]. However, we find that the point-based query strategy in TriplaneGaussian cannot fully fetch valuable features from the spherical triplane. Therefore, we analyze the inner rendering mechanism of spherical triplane and propose a novel ray-based

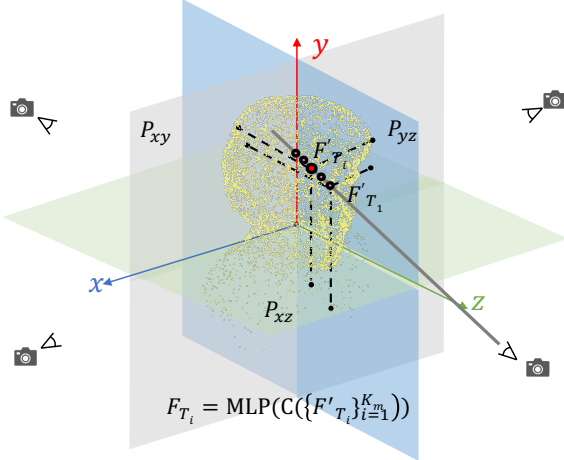


Figure 3. The proposed feature aggregation mechanism samples and aggregates multi-layer features from the spherical triplane for each point.

sampling strategy to aggregate multiple layers of features effectively. Specifically, we initialize the $H_T \times W_T \times 6 \times C_t$ spherical triplane features with learnable query features, which are then flattened into spherical triplane token features $F_T \in \mathbb{R}^{N_T \times C_t}$, where $N_T = H_T \times W_T \times 6$. These learnable features then interact with the image features F_I with stacked cross-attention blocks $\mathcal{A}_T = \{\mathcal{A}_{T_i}\}_{i=1}^{L_{\mathcal{A}_T}}$ similar to the learnable point features as:

$$F_{T_i} = \mathcal{A}_{T_i}(F_{T_{i-1}}, F_I), \quad (9)$$

where F_{T_i} is the i_{th} layer of spherical triplane features in the stacked cross-attention layers. The final output features are then projected by MLPs to the same channel as the spherical triplane in SphereHead. We then need to query the feature from the spherical triplane to enhance the point features. One vanilla way is to follow TriplaneGaussian and use our densified point cloud to fetch the corresponding feature by projection. However, we find that our point clouds are distributed on the shape surface similar to a mesh, and such a single-layer query strategy cannot fully aggregate the corresponding features of each point from the spherical triplane. That's because the triplane designed for NeRF-based rendering requires ray marching to aggregate multiple points(layers) of features for rendering. Using a single point cloud on the shape surface cannot fully fetch valuable features from the spherical triplane. While ray marching is computationally consuming and inefficient, we propose to sample multiple layers of points from the single-layer point cloud for feature aggregation. Specifically, we sample 4 virtual cameras that can capture the front, left, right, and back sides of the head. As is shown in Fig. 3, for each camera, we cast a ray from the camera center to each point P_i , then K_m number of points $P'_i = \{P'_i\}_{i=1}^{K_m}$ are sampled along the

ray near the point. Each point then queries features from the spherical triplane by projection. We then concatenate and aggregate these queried features with MLPs to obtain the final spherical triplane features as:

$$F_{T_i} = \text{MLP}(\mathcal{C}(\{F'_{T_i}\}_{i=1}^{K_m})), \quad (10)$$

where F'_{T_i} is the spherical triplane feature queried by sampled point P'_i ; \mathcal{C} is the concatenation operation; and F_{T_i} is the final aggregated feature for point P_i . In this way, each point gets its aggregated spherical triplane feature. These aggregated spherical triplane features can be concatenated with the point feature for dense Gaussian attribute regression as in Formula (8).

To supervise this branch in distilling the knowledge from SphereHead, we add the frozen decoding header from SphereHead to decode the spherical triplane feature to the target image and supervise it with the ground truth image during training. Specifically, as shown in the bottom right part of Fig. 2, for each target view, we project the point feature to the image plane by the Gaussian rasterizer and then use the frozen decoder from SphereHead to decode the target image from the projected spherical triplane features.

3.4. Large-scale Training Data Generation

The scale of the training dataset is also a key factor in enabling the generalizability of a trained model. However, obtaining a large dataset with diverse head assets is challenging. Though various datasets have been proposed for 3D head modeling, as shown in Table 1, they have limited diversity of subjects, which hinders the generalization capability of learning-based models. Inspired by previous methods [8, 28, 62, 78] in various fields that model trained from synthesis data can generalize to real-world scenarios during inference, we leverage pretrained priors from 3D GANs and generate a large-scale, diverse dataset for training. Specifically, we leverage two prior models for data generation, EG3D for multiview front face images synthesis, and SphereHead for 360° view images generation. Our observation is that the EG3D generates a different distribution of images compared to SphereHead (e.g., diverse hairstyles and caps appeared in samples), while SphereHead is able to generate 360° images. The combination of two model spaces enlarges the diversity of the generated images and empowers better generalizability for learning-based models. However, bad cases may occur in the generated dataset, which can hurt the model. Therefore, we remove bad cases from the sampled images manually, ending up with 48,135 subjects in Ours-Front and 117,186 subjects in Ours-360 datasets.

3.5. Optimization and Regularization

In the training phase, we randomly select N_v different views of images rendered from the same triplane. We ran-

domly choose one as the reference image for the Gaussian full-head reconstruction, while the others serve as novel view images for prediction and training. Note that the two branches in our framework both render images for supervision. We ensure the accuracy of the rendered RGB images from each branch by comparing them with the ground truth target images, utilizing a combination of \mathcal{L}_1 loss and perceptual loss for supervision.

$$\mathcal{L}_{rgb} = \lambda_1 \mathcal{L}_1 + \lambda_2 \mathcal{L}_{lpips}. \quad (11)$$

Additionally, for the sparse and dense Gaussian Splatting branch, we render the silhouette and supervise it using \mathcal{L}_1 loss, referred to as \mathcal{L}_{mask} . And for the spherical triplane branch, we supervise the extracted triplane feature with the triplane feature in the pretrained SphereHead with \mathcal{L}_1 loss, denoted as \mathcal{L}_{tri} . The total loss function is a weighted sum as:

$$\mathcal{L} = \lambda_3 \mathcal{L}_{rgb}^G + \lambda_4 \mathcal{L}_{rgb}^T + \lambda_5 \mathcal{L}_{mask} + \lambda_6 \mathcal{L}_{tri}, \quad (12)$$

where \mathcal{L}_{rgb}^G denotes the RGB image loss for both sparse and dense Gaussian Splatting and \mathcal{L}_{rgb}^T for the auxiliary triplane branch, both denoted as in Formula (11).

4. Experiments

4.1. Experiments Setting

Implementation Details. Our framework is implemented using PyTorch, with the DINoV2 image feature extraction backbone frozen. The Transformer component comprises 10 layers of basic blocks, featuring 16 attention heads and a feature dimension of 1024 ($C_t = 1024$). The extracted features are translated into Gaussian attributes through three multilayer perceptron (MLP) layers. The training of the network is conducted over 100 epochs using the Adam optimizer and a cosine warm-up scheduler. Various hyperparameters are empirically set to optimize performance, including $N_v = 6$, $\lambda_1 = \lambda_2 = 1.0$, $\lambda_3 = 1.0$, $\lambda_4 = 0.1$, $\lambda_5 = 1.0$, $\lambda_6 = 0.0001$, $\epsilon_{O_C} = 0.15$, $\epsilon_{O_D} = 0.056$, $M_D = 10K$, $K_m = 32$, $\lambda_{area} = 2.0e-6$, $H_T = W_T = 64$.

Datasets. For our training and testing, we employ the large-scale dataset that we have generated. To assess the 360-degree synthesis capability, we randomly select 100 subjects from our Ours-360 dataset for testing, and the remaining for training.

Evaluation Metrics. We evaluate the quality of our synthesized images using three quantitative metrics: Peak Signal-to-Noise Ratio (PSNR), Structural Similarity Index (SSIM), and Learned Perceptual Image Patch Similarity (LPIPS). These measures enable us to effectively compare

Table 2. Running time for 3D head avatar generation from a single input image and rendering a 3D representation. PH-PTI denotes PanoHead-PTI, and SH-PTI denotes SphereHead-PTI.

Time	H.NeRF	EG3D-PTI	PH-PTI	SH-PTI	Ours
Reconstruction	60s	120s	89.4s	96.2s	0.11s
Render	58ms	24ms	10.29ms	19.68ms	1.4ms

Table 3. Quantitative evaluation on the 100-person testset.

Method	PSNR \uparrow	LPIPS \downarrow	SSIM \uparrow	APD \downarrow	CSIM \uparrow
PanoHead-PTI	16.260	0.165	0.704	0.029	0.680
SphereHead-PTI	16.983	0.142	0.698	0.018	0.808
LGM	11.472	0.444	0.572	0.102	0.457
Ours	23.494	0.107	0.793	0.015	0.790

the synthetic images with the ground truth, ensuring a comprehensive assessment of the reconstruction quality. To evaluate identity similarity (CSIM) of the reconstructed 3D assets, we compute the cosine distance of face recognition features, building on the work of [20]. For assessing pose fidelity, we employ the Average Pose Distance (APD) [21].

4.2. Main Results

Qualitative Results. Fig. 9 and Fig. 10 illustrate the novel view synthesis results after reconstruction from various methods, highlighting the superior performance of PanoLAM. Unlike prior approaches, PanoLAM enhances texture detail, maintains identity fidelity, and ensures multiview consistency. Due to the subtlety of multiview consistency in static images, we encourage viewing our supplementary video for a clearer demonstration. It is noteworthy that PanoLAM neither employs time-intensive test-time optimization nor relies on precise camera poses for accurate reconstruction, showcasing the efficacy of our pose-free framework. We achieve these results with 800X speedup.

Quantitative Results. We benchmark our framework and baselines on the test set. For each subject, we evaluate 4 viewpoints: the front, back, left, and right. For the baseline method, we use their default configuration. As presented in Table 3, Our PanoLAM demonstrates exceptional reconstruction quality according to PSNR, SSIM, and LPIPS metrics. Furthermore, CSIM metrics indicate strong identity consistency of our methods. Remarkably, these achievements are coupled with fast reconstruction and rendering speeds, underscoring the effectiveness and efficiency of our approach.

Reconstruction and Render Speed on Various Platforms. Table 2 shows the comparative running time evaluation of all methods on an A100 GPU. Benefiting from our

coarse-to-fine and feedforward framework design, our approach achieves a fast reconstruction speed. The Gaussian Splatting we chose as the 3D representation also enables fast rendering speeds compared to existing techniques.

Analysis of Feature Sampling and Aggregation Mechanism from Spherical Triplane. We analyze the feature aggregation mechanism from the spherical triplane of SphereHead to explore a better knowledge distillation strategy. In Fig. 7, we cast rays and visualize the aggregation weights of each sampled feature in the original ray marching. We plot 4 curves showing the weight values of 4 casting rays. As shown in the figure, multiple peaks occur near the geometry surface hit by each ray, indicating that we need to sample and aggregate multiple points on a ray to fetch valuable features from the spherical triplane fully. Moreover, each weight curve appears to be a different weight function, indicating that we cannot apply the same manual weight functions, e.g., a Gaussian distribution, for each ray. Thereafter, we propose to leverage learnable MLPs to learn the feature aggregation function from large-scale data. Experimental results in the ablation study validate such a finding and the effectiveness of our design.

4.3. Ablation Studies

Effect of Different Number of Gaussian Points. Fig. 5 ablates the effect of different numbers of Gaussian points. As is shown in the figure, less number of Gaussian points are not able to reconstruct details like hair-strands and mustaches well, leading to blurry results in these regions.

Effect of Coarse-to-fine Gaussian Point Generation. In Fig. 4, we visualize the effect of our coarse-to-fine Gaussian generation strategy. As is shown in the figure, the sparse points are easier to optimize and can be easily deformed to carve the shape of the person. However, a small number of Gaussian points cannot model texture details like hair strands. By leveraging the topology prior in the FLAME mesh, we effectively densify the points to learn more detailed textures. In contrast, directly predicting and regressing the dense point cloud results in insufficient optimization of Gaussian points. Many points are not well optimized for deformation and remain on the FLAME surface, which are invisible and wasted, causing dual-layer geometry in the hair region as well. Moreover, our coarse-to-fine strategy saves computation and GPU memory consumption since fewer points are needed for stacked cross-attention modules, which is shown in Table 4.

Effect of Different Dataset Scale. Previous 3D head datasets lack subject diversity, as shown in Table 1. We ablate the effect of different numbers of subjects in Fig. 6. We keep all other configures the same and train our model with

Table 4. Ablation on our coarse-to-fine generation strategy on different numbers of Gaussian points. OOM denotes out of memory for an 80G GPU, and - denotes no results.

Metrics	5K	D-30K	C2F-30K	D-100K	C2F-100K
Inference Time↓	0.071s	0.49s	0.082s	-	0.11s
GPU Memory↓	5.77G	17.1G	7.22G	OOM	12.7G
Training Time (Batch=1)↓	0.39s	0.94s	0.51s	-	0.77s

different numbers of subjects. We infer all models with the same testing subjects. The model trained on a limited number of subjects can not generalize well to unseen subjects, showing the effectiveness of our proposed large-scale, diverse dataset for network generalizability.

Effect of Different Spherical Triplane Query Strategy. In Fig. 8, we show the results of different query strategies from the spherical triplane. All strategies use the same feature renderer and frozen decoder from SphereHead for target image decoding. As shown in the figure, directly using the densified point cloud to query a single layer of features from the spherical triplane, as in [96], cannot fetch all valuable features, and the rendered images contain artifacts due to missing information. We then add 4 virtual cameras and cast rays from the camera center to each point and sample 32 layers of features near the point surface for feature aggregation. We set the margin between each sampled point to be the same as the fine ray marching stage in SphereHead. We try to assign manual weights sampled from a normal distribution centered at the selected point with standard deviation 1 and 10, and aggregate sampled features with a weighted sum. As is shown in the middle part of Fig. 8, the results look better but are still blurry. Our final solution utilizes learnable MLPs to learn the aggregation function for the NeRF-based rendering. As shown in the figure, ours gets the best results, showing the effectiveness of the proposed aggregation strategy.

5. Conclusions

In this work, we present a novel feedforward large avatar model for Gaussian full-head synthesis from a single unposed image. To resolve the problem of lacking 3D assets for network training, we develop a large-scale, diverse 3D avatar dataset from trained 3D GANs. We also propose a coarse-to-fine mechanism with a network-free point cloud densification strategy for efficient reconstruction of a high-fidelity Gaussian full-head from a single image. We also introduce a dual-branch approach to distill knowledge from the spherical triplane prior and improve the reconstruction effectiveness. We analyze the feature sampling mechanism in spherical triplane and propose an efficient aggregation mechanism. Experimental results validate the effectiveness of our approach.

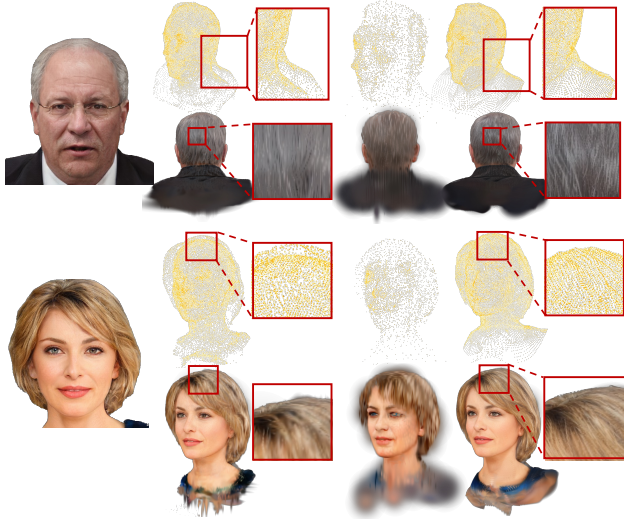


Figure 4. Comparison of our coarse-to-fine generation and direct dense generation. Without the coarse-to-fine strategy, the dense Gaussians are distributed on multiple layers, leading to degradation of rendering quality. Zoom in for details.



Figure 5. Comparison of different numbers of Gaussian points. A small number of Gaussian points cannot model texture details like hair strands and teeth. More high-fidelity avatars are reconstructed with an increasing number of Gaussian points. Zoom in to see more details.

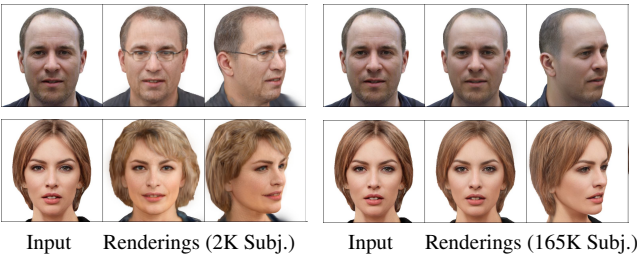


Figure 6. Comparison of our network trained on different numbers of subjects. The model trained on a small number of subjects cannot generalize well to unseen identities.

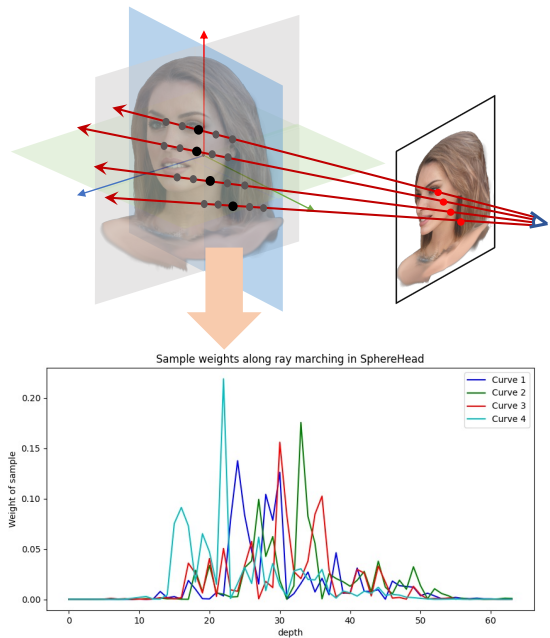


Figure 7. Analysis of ray marching aggregation weights in the original Spherical Triplane in SphereHead. We cast rays and visualize the aggregation weights of each sampled feature in the original ray marching process. Two phenomena occur. Firstly, multiple peaks occur near the geometry surface hit by each ray in each curve, indicating that multiple layers of features should be aggregated rather than a single query to access the full valuable information residing in the spherical triplane. Secondly, each curve appears to be a different weight function. Thereafter, learning-based approaches, e.g., MLPs, can better model this aggregation operation.



Figure 8. Comparisons on different spherical triplane feature query and aggregation strategies. For each point, sampling only one sample of features from the spherical triplane cannot fully fetch all valuable features, resulting in a collapsed rendered image. Aggregating 32 points with Gaussian distribution weights gets better results, but still blurry. Our MLPs learn to aggregate features as the original NeRF and get quite better results.

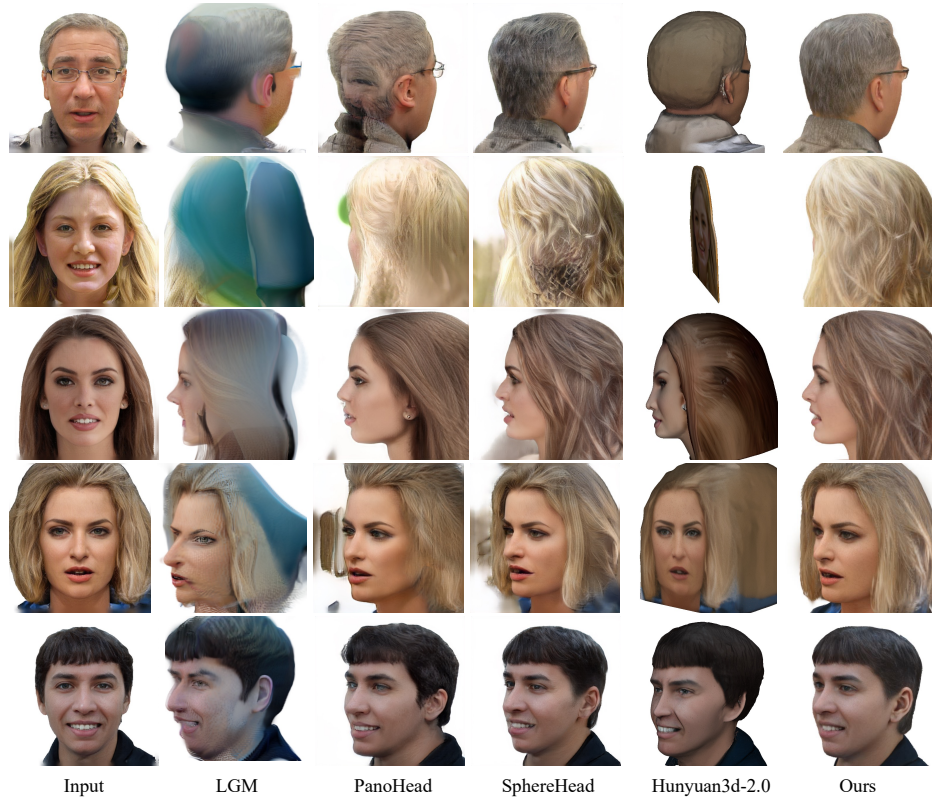


Figure 9. Comparison of reconstruction and novel view synthesis of different methods on the testset.

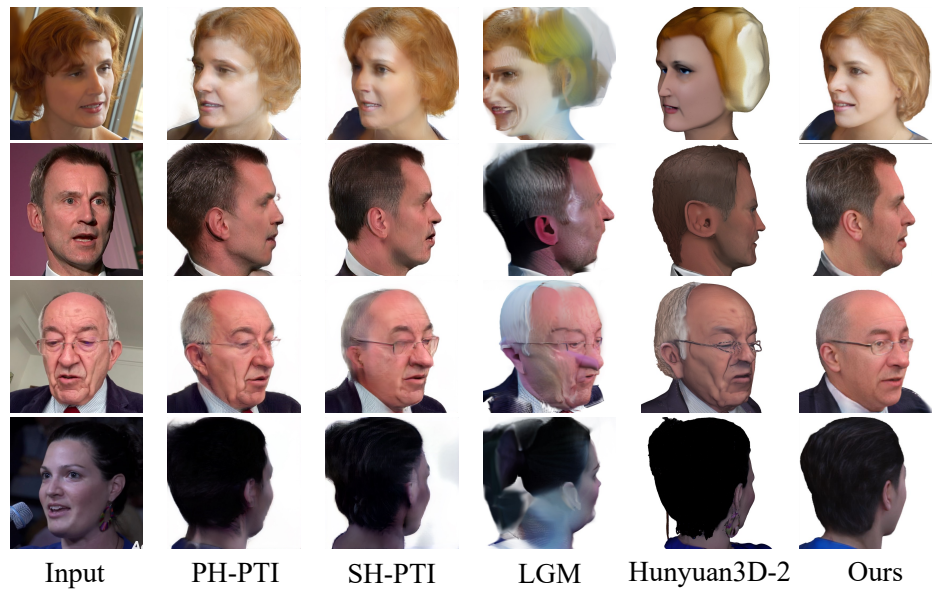


Figure 10. Comparison of reconstruction and novel view synthesis of different methods on real-world in-the-wild images.

References

[1] Rameen Abdal, Yifan Wang, Zifan Shi, Yinghao Xu, Ryan Po, Zhengfei Kuang, Qifeng Chen, Dit-Yan Yeung, and Gordon Wetzstein. Gaussian shell maps for efficient 3d human generation. In *IEEE/CVF Conference on Computer Vision and Pattern Recognition, CVPR 2024, Seattle, WA, USA, June 16-22, 2024*, pages 9441–9451. IEEE, 2024. 3

[2] Sizhe An, Hongyi Xu, Yichun Shi, Guoxian Song, Ümit Y. Ogras, and Linjie Luo. Panohead: Geometry-aware 3d full-head synthesis in 360°. In *IEEE/CVF Conference on Computer Vision and Pattern Recognition, CVPR 2023, Vancouver, BC, Canada, June 17-24, 2023*, pages 20950–20959. IEEE, 2023. 2, 3

[3] ShahRukh Athar, Zexiang Xu, Kalyan Sunkavalli, Eli Shechtman, and Zhixin Shu. Rignerf: Fully controllable neural 3d portraits. In *IEEE/CVF Conference on Computer Vision and Pattern Recognition, CVPR 2022, New Orleans, LA, USA, June 18-24, 2022*, pages 20332–20341. IEEE, 2022. 2

[4] Yunpeng Bai, Yanbo Fan, Xuan Wang, Yong Zhang, Jingxiang Sun, Chun Yuan, and Ying Shan. High-fidelity facial avatar reconstruction from monocular video with generative priors. In *IEEE/CVF Conference on Computer Vision and Pattern Recognition, CVPR 2023, Vancouver, BC, Canada, June 17-24, 2023*, pages 4541–4551. IEEE, 2023.

[5] Ziqian Bai, Feitong Tan, Zeng Huang, Kripasindhu Sarkar, Danhang Tang, Di Qiu, Abhimitra Meka, Ruofei Du, Mingsong Dou, Sergio Orts-Escalano, Rohit Pandey, Ping Tan, Thabo Beeler, Sean Fanello, and Yinda Zhang. Learning personalized high quality volumetric head avatars from monocular RGB videos. In *IEEE/CVF Conference on Computer Vision and Pattern Recognition, CVPR 2023, Vancouver, BC, Canada, June 17-24, 2023*, pages 16890–16900. IEEE, 2023. 2

[6] Ananta R. Bhattacharai, Matthias Nießner, and Artem Sevestopolsky. Triplanenet: An encoder for EG3D inversion. In *IEEE/CVF Winter Conference on Applications of Computer Vision, WACV 2024, Waikoloa, HI, USA, January 3-8, 2024*, pages 3043–3053. IEEE, 2024. 3

[7] Volker Blanz and Thomas Vetter. A morphable model for the synthesis of 3d faces. In *Proceedings of the 26th Annual Conference on Computer Graphics and Interactive Techniques, SIGGRAPH 1999, Los Angeles, CA, USA, August 8-13, 1999*, pages 187–194. ACM, 1999. 2

[8] Junhao Cai, Yisheng He, Weihao Yuan, Siyu Zhu, Zilong Dong, Liefeng Bo, and Qifeng Chen. Open-vocabulary category-level object pose and size estimation. *IEEE Robotics and Automation Letters*, 2024. 6

[9] Antonio Canela, Pol Caselles, Ibrar Malik, Eduard Ramon, Jaime García, Jordi Sanchez-Riera, Gil Triginer, and Francesc Moreno-Noguer. Instantavatar: Efficient 3d head reconstruction via surface rendering. In *International Conference on 3D Vision, 3DV 2024, Davos, Switzerland, March 18-21, 2024*, pages 995–1005. IEEE, 2024. 2

[10] Chen Cao, Yanlin Weng, Shun Zhou, Yiyi Tong, and Kun Zhou. Facewarehouse: A 3d facial expression database for visual computing. *IEEE Trans. Vis. Comput. Graph.*, 20(3):413–425, 2014. 3

[11] Eric R Chan, Connor Z Lin, Matthew A Chan, Koki Nagano, Boxiao Pan, Shalini De Mello, Orazio Gallo, Leonidas J Guibas, Jonathan Tremblay, Sameh Khamis, et al. Efficient geometry-aware 3d generative adversarial networks. In *Proceedings of the IEEE/CVF conference on computer vision and pattern recognition*, pages 16123–16133, 2022. 2, 3

[12] Eric R. Chan, Connor Z. Lin, Matthew A. Chan, Koki Nagano, Boxiao Pan, Shalini De Mello, Orazio Gallo, Leonidas J. Guibas, Jonathan Tremblay, Sameh Khamis, Tero Karras, and Gordon Wetzstein. Efficient geometry-aware 3d generative adversarial networks. In *IEEE/CVF Conference on Computer Vision and Pattern Recognition, CVPR 2022, New Orleans, LA, USA, June 18-24, 2022*, pages 16102–16112. IEEE, 2022. 3

[13] Xingyu Chen, Yu Deng, and Baoyuan Wang. Mimic3d: Thriving 3d-aware gans via 3d-to-2d imitation. In *IEEE/CVF International Conference on Computer Vision, ICCV 2023, Paris, France, October 1-6, 2023*, pages 2338–2348. IEEE, 2023. 3

[14] Yufan Chen, Lizhen Wang, Qijing Li, Hongjiang Xiao, Shengping Zhang, Hongxun Yao, and Yebin Liu. Monogaussianavatar: Monocular gaussian point-based head avatar. In *ACM SIGGRAPH 2024 Conference Papers, SIGGRAPH 2024, Denver, CO, USA, 27 July 2024- 1 August 2024*, page 58. ACM, 2024. 2

[15] Shiyang Cheng, Irene Kotsia, Maja Pantic, and Stefanos Zafeiriou. 4dfab: A large scale 4d database for facial expression analysis and biometric applications. In *2018 IEEE Conference on Computer Vision and Pattern Recognition, CVPR 2018, Salt Lake City, UT, USA, June 18-22, 2018*, pages 5117–5126. Computer Vision Foundation / IEEE Computer Society, 2018. 3

[16] Xuangeng Chu and Tatsuya Harada. Generalizable and animatable gaussian head avatar. In *Advances in Neural Information Processing Systems 38: Annual Conference on Neural Information Processing Systems 2024, NeurIPS 2024, Vancouver, BC, Canada, December 10 - 15, 2024*, 2024. 3

[17] Xuangeng Chu, Yu Li, Ailing Zeng, Tianyu Yang, Lijian Lin, Yunfei Liu, and Tatsuya Harada. Gpavatar: Generalizable and precise head avatar from image(s). In *The Twelfth International Conference on Learning Representations, ICLR 2024, Vienna, Austria, May 7-11, 2024*. OpenReview.net, 2024. 3

[18] Darren Cosker, Eva Krumhuber, and Adrian Hilton. A FACS valid 3d dynamic action unit database with applications to 3d dynamic morphable facial modeling. In *IEEE International Conference on Computer Vision, ICCV 2011, Barcelona, Spain, November 6-13, 2011*, pages 2296–2303. IEEE Computer Society, 2011. 3

[19] Hang Dai, Nick E. Pears, William A. P. Smith, and Christian Duncan. Statistical modeling of craniofacial shape and texture. *Int. J. Comput. Vis.*, 128(2):547–571, 2020. 3

[20] Jiankang Deng, Jia Guo, Jing Yang, Niannan Xue, Irene Kotsia, and Stefanos Zafeiriou. Arcface: Additive angular margin loss for deep face recognition. *IEEE Trans. Pattern Anal. Mach. Intell.*, 44(10):5962–5979, 2022. 7

[21] Yu Deng, Jiaolong Yang, Sicheng Xu, Dong Chen, Yunde Jia, and Xin Tong. Accurate 3d face reconstruction with

weakly-supervised learning: From single image to image set. In *IEEE Conference on Computer Vision and Pattern Recognition Workshops, CVPR Workshops 2019, Long Beach, CA, USA, June 16-20, 2019*, pages 285–295. Computer Vision Foundation / IEEE, 2019. 7

[22] Yu Deng, Duomin Wang, and Baoyuan Wang. Portrait4d-v2: Pseudo multi-view data creates better 4d head synthesizer. In *Computer Vision - ECCV 2024 - 18th European Conference, Milan, Italy, September 29-October 4, 2024, Proceedings, Part XVII*, pages 316–333. Springer, 2024. 3

[23] Helisa Dhamo, Yinyu Nie, Arthur Moreau, Jifei Song, Richard Shaw, Yiren Zhou, and Eduardo Pérez-Pellitero. Headgas: Real-time animatable head avatars via 3d gaussian splatting. In *Computer Vision - ECCV 2024 - 18th European Conference, Milan, Italy, September 29-October 4, 2024, Proceedings, Part II*, pages 459–476. Springer, 2024. 2

[24] Matheus Gadelha, Subhransu Maji, and Rui Wang. 3d shape induction from 2d views of multiple objects. In *2017 International Conference on 3D Vision, 3DV 2017, Qingdao, China, October 10-12, 2017*, pages 402–411. IEEE Computer Society, 2017. 3

[25] Guy Gafni, Justus Thies, Michael Zollhöfer, and Matthias Nießner. Dynamic neural radiance fields for monocular 4d facial avatar reconstruction. In *IEEE Conference on Computer Vision and Pattern Recognition, CVPR 2021, virtual, June 19-25, 2021*, pages 8649–8658. Computer Vision Foundation / IEEE, 2021. 2

[26] Xuan Gao, Chenglai Zhong, Jun Xiang, Yang Hong, Yudong Guo, and Juyong Zhang. Reconstructing personalized semantic facial nerf models from monocular video. *ACM Trans. Graph.*, 41(6):200:1–200:12, 2022.

[27] Yudong Guo, Keyu Chen, Sen Liang, Yong-Jin Liu, Hujun Bao, and Juyong Zhang. Ad-nerf: Audio driven neural radiance fields for talking head synthesis. In *2021 IEEE/CVF International Conference on Computer Vision, ICCV 2021, Montreal, QC, Canada, October 10-17, 2021*, pages 5764–5774. IEEE, 2021. 2

[28] Yisheng He, Yao Wang, Haoqiang Fan, Jian Sun, and Qifeng Chen. Fs6d: Few-shot 6d pose estimation of novel objects. In *Proceedings of the IEEE/CVF Conference on Computer Vision and Pattern Recognition*, pages 6814–6824, 2022. 6

[29] Yuxiao He, Yiyu Zhuang, Yanwen Wang, Yao Yao, Siyu Zhu, Xiaoyu Li, Qi Zhang, Xun Cao, and Hao Zhu. Head360: Learning a parametric 3d full-head for free-view synthesis in 360°. In *Computer Vision - ECCV 2024 - 18th European Conference, Milan, Italy, September 29-October 4, 2024, Proceedings, Part LVI*, pages 254–272. Springer, 2024. 3

[30] Yisheng He, Xiaodong Gu, Xiaodan Ye, Chao Xu, Zhengyi Zhao, Yuan Dong, Weihao Yuan, Zilong Dong, and Liefeng Bo. LAM: large avatar model for one-shot animatable gaussian head. In *ACM SIGGRAPH 2025 Conference Proceedings*, 2025. 3, 4

[31] Yang Hong, Bo Peng, Haiyao Xiao, Ligang Liu, and Juyong Zhang. Headnerf: A real-time nerf-based parametric head model. *CoRR*, abs/2112.05637, 2021. 2

[32] Yuxiao Hu, ZhenQiu Zhang, Xun Xu, Yun Fu, and Thomas S. Huang. Building large scale 3d face database for face analysis. In *Multimedia Content Analysis and Mining, International Workshop, MCAM 2007, Weihai, China, June 30 - July 1, 2007, Proceedings*, pages 343–350. Springer, 2007. 3

[33] Tero Karras, Samuli Laine, and Timo Aila. A style-based generator architecture for generative adversarial networks. In *IEEE Conference on Computer Vision and Pattern Recognition, CVPR 2019, Long Beach, CA, USA, June 16-20, 2019*, pages 4401–4410. Computer Vision Foundation / IEEE, 2019. 2

[34] Vahid Kazemi and Josephine Sullivan. One millisecond face alignment with an ensemble of regression trees. In *2014 IEEE Conference on Computer Vision and Pattern Recognition, CVPR 2014, Columbus, OH, USA, June 23-28, 2014*, pages 1867–1874. IEEE Computer Society, 2014. 16

[35] Bernhard Kerbl, Georgios Kopanas, Thomas Leimkühler, and George Drettakis. 3d gaussian splatting for real-time radiance field rendering. *ACM Trans. Graph.*, 42(4):139:1–139:14, 2023. 2, 3

[36] Taras Khakhulin, Vanessa Sklyarova, Victor Lempitsky, and Egor Zakharov. Realistic one-shot mesh-based head avatars. In *Computer Vision - ECCV 2022 - 17th European Conference, Tel Aviv, Israel, October 23-27, 2022, Proceedings, Part II*, pages 345–362. Springer, 2022. 2

[37] Taekyung Ki, Dongchan Min, and Gyeongsu Chae. Learning to generate conditional tri-plane for 3d-aware expression controllable portrait animation. In *Computer Vision - ECCV 2024 - 18th European Conference, Milan, Italy, September 29-October 4, 2024, Proceedings, Part I*, pages 476–493. Springer, 2024. 2

[38] Taewoo Kim, Chaeyeon Chung, Sunghyun Park, Gyojung Gu, Keonmin Nam, Wonzo Choe, Jaesung Lee, and Jaegul Choo. K-hairstyle: A large-scale korean hairstyle dataset for virtual hair editing and hairstyle classification. In *2021 IEEE International Conference on Image Processing, ICIP 2021, Anchorage, AK, USA, September 19-22, 2021*, pages 1299–1303. IEEE, 2021. 16

[39] Tobias Kirschstein, Shenhan Qian, Simon Giebenhain, Tim Walter, and Matthias Nießner. Nersemble: Multi-view radiance field reconstruction of human heads. *ACM Trans. Graph.*, 42(4), 2023. 3

[40] Tobias Kirschstein, Simon Giebenhain, Jiapeng Tang, Markos Georgopoulos, and Matthias Nießner. Gghead: Fast and generalizable 3d gaussian heads. In *SIGGRAPH Asia 2024 Conference Papers, SA 2024, Tokyo, Japan, December 3-6, 2024*, pages 126:1–126:11. ACM, 2024. 3

[41] Tobias Kirschstein, Javier Romero, Artem Sevastopolsky, Matthias Nießner, and Shunsuke Saito. Avat3r: Large animatable gaussian reconstruction model for high-fidelity 3d head avatars. *CoRR*, abs/2502.20220, 2025. 3

[42] Jaehoon Ko, Kyusun Cho, Daewon Choi, Kwangrok Ryoo, and Seungryong Kim. 3d GAN inversion with pose optimization. In *IEEE/CVF Winter Conference on Applications of Computer Vision, WACV 2023, Waikoloa, HI, USA, January 2-7, 2023*, pages 2966–2975. IEEE, 2023. 2, 3

[43] Heyuan Li, Ce Chen, Tianhao Shi, Yuda Qiu, Sizhe An, Guanying Chen, and Xiaoguang Han. Spherehead: Stable 3d full-head synthesis with spherical tri-plane representation. In *Computer Vision - ECCV 2024 - 18th European Conference, Milan, Italy, September 29-October 4, 2024, Proceedings, Part LXXV*, pages 324–341. Springer, 2024. 2, 3, 5, 16

[44] Ruihui Li, Xianzhi Li, Pheng-Ann Heng, and Chi-Wing Fu. Point cloud upsampling via disentangled refinement. In *IEEE Conference on Computer Vision and Pattern Recognition, CVPR 2021, virtual, June 19-25, 2021*, pages 344–353. Computer Vision Foundation / IEEE, 2021. 5

[45] Tianye Li, Timo Bolkart, Michael J. Black, Hao Li, and Javier Romero. Learning a model of facial shape and expression from 4d scans. *ACM Trans. Graph.*, 36(6):194:1–194:17, 2017. 2

[46] Weichuang Li, Longhao Zhang, Dong Wang, Bin Zhao, Zhi-gang Wang, Mulin Chen, Bang Zhang, Zhongjian Wang, Liefeng Bo, and Xuelong Li. One-shot high-fidelity talking-head synthesis with deformable neural radiance field. In *IEEE/CVF Conference on Computer Vision and Pattern Recognition, CVPR 2023, Vancouver, BC, Canada, June 17-24, 2023*, pages 17969–17978. IEEE, 2023. 2

[47] Xuetong Li, Shalini De Mello, Sifei Liu, Koki Nagano, Umar Iqbal, and Jan Kautz. Generalizable one-shot 3d neural head avatar. In *Advances in Neural Information Processing Systems 36: Annual Conference on Neural Information Processing Systems 2023, NeurIPS 2023, New Orleans, LA, USA, December 10 - 16, 2023*, 2023. 3

[48] Tingting Liao, Yujian Zheng, Adilbek Karmanov, Liwen Hu, Leyang Jin, Yuliang Xiu, and Hao Li. Soap: Style-omniscient animatable portraits. In *ACM SIGGRAPH 2025 Conference Proceedings*, 2025. 2

[49] Yiyi Liao, Katja Schwarz, Lars M. Mescheder, and Andreas Geiger. Towards unsupervised learning of generative models for 3d controllable image synthesis. In *2020 IEEE/CVF Conference on Computer Vision and Pattern Recognition, CVPR 2020, Seattle, WA, USA, June 13-19, 2020*, pages 5870–5879. Computer Vision Foundation / IEEE, 2020. 3

[50] Ziwei Liu, Ping Luo, Xiaogang Wang, and Xiaou Tang. Deep learning face attributes in the wild. In *2015 IEEE International Conference on Computer Vision, ICCV 2015, Santiago, Chile, December 7-13, 2015*, pages 3730–3738. IEEE Computer Society, 2015. 16

[51] Shengjie Ma, Yanlin Weng, Tianjia Shao, and Kun Zhou. 3d gaussian blendshapes for head avatar animation. In *ACM SIGGRAPH 2024 Conference Papers, SIGGRAPH 2024, Denver, CO, USA, 27 July 2024- 1 August 2024*, page 60. ACM, 2024. 2

[52] Zhiyuan Ma, Xiangyu Zhu, Guojun Qi, Zhen Lei, and Lei Zhang. Otavatar: One-shot talking face avatar with controllable tri-plane rendering. In *IEEE/CVF Conference on Computer Vision and Pattern Recognition, CVPR 2023, Vancouver, BC, Canada, June 17-24, 2023*, pages 16901–16910. IEEE, 2023. 2

[53] Julieta Martinez, Emily Kim, Javier Romero, Timur M. Bagautdinov, Shunsuke Saito, Shouo-I Yu, Stuart Anderson, Michael Zollhöfer, Te-Li Wang, Shaojie Bai, Chenghui Li, Shih-En Wei, Rohan Joshi, Wyatt Borsos, Tomas Simon, Jason M. Saragih, Paul Theodosis, Alexander Greene, Anjani Josyula, Silvio Maeta, Andrew Jewett, Simion Venshtain, Christopher Heilman, Yueh-Tung Chen, Sidi Fu, Mohamed Elshaer, Tingfang Du, Longhua Wu, Shen-Chi Chen, Kai Kang, Michael Wu, Youssef Emad, Steven Longay, Ashley Brewer, Hitesh Shah, James Booth, Taylor Koska, Kayla Hidle, Matthew Andromalos, Joanna Hsu, Thomas Dauer, Peter Selednik, Timothy Godisart, Scott Ardisson, Matthew Cipperly, Ben Humberston, Lon Farr, Bob Hansen, Peihong Guo, Dave Braun, Steven Krenn, He Wen, Lucas Evans, Natalia Fadeeva, Matthew Stewart, Gabriel Schwartz, Divam Gupta, Gyeongsik Moon, Kaiwen Guo, Yuan Dong, Yichen Xu, Takaaki Shiratori, Fabian Prada, Bernardo Pires, Bo Peng, Julia Buffalini, Autumn Trimble, Kevyn McPhail, Melissa Schoeller, and Yaser Sheikh. Codec avatar studio: Paired human captures for complete, driveable, and generalizable avatars. In *Advances in Neural Information Processing Systems 38: Annual Conference on Neural Information Processing Systems 2024, NeurIPS 2024, Vancouver, BC, Canada, December 10 - 15, 2024*, 2024. 3

[54] Ben Mildenhall, Pratul P. Srinivasan, Matthew Tancik, Jonathan T. Barron, Ravi Ramamoorthi, and Ren Ng. Nerf: Representing scenes as neural radiance fields for view synthesis. In *Computer Vision - ECCV 2020 - 16th European Conference, Glasgow, UK, August 23-28, 2020, Proceedings, Part I*, pages 405–421. Springer, 2020. 2, 4

[55] Thu Nguyen-Phuoc, Chuan Li, Lucas Theis, Christian Richardt, and Yong-Liang Yang. Hologan: Unsupervised learning of 3d representations from natural images. In *2019 IEEE/CVF International Conference on Computer Vision, ICCV 2019, Seoul, Korea (South), October 27 - November 2, 2019*, pages 7587–7596. IEEE, 2019. 3

[56] Thu Nguyen-Phuoc, Christian Richardt, Long Mai, Yong-Liang Yang, and Niloy J. Mitra. Blockgan: Learning 3d object-aware scene representations from unlabelled images. In *Advances in Neural Information Processing Systems 33: Annual Conference on Neural Information Processing Systems 2020, NeurIPS 2020, December 6-12, 2020, virtual*, 2020. 3

[57] Maxime Oquab, Timothée Darcet, Théo Moutakanni, Huy V. Vo, Marc Szafraniec, Vasil Khalidov, Pierre Fernandez, Daniel Haziza, Francisco Massa, Alaaeldin El-Nouby, Mido Assran, Nicolas Ballas, Wojciech Galuba, Russell Howes, Po-Yao Huang, Shang-Wen Li, Ishan Misra, Michael Rabat, Vasu Sharma, Gabriel Synnaeve, Hu Xu, Hervé Jégou, Julien Mairal, Patrick Labatut, Armand Joulin, and Piotr Bojanowski. Dinov2: Learning robust visual features without supervision. *Trans. Mach. Learn. Res.*, 2024, 2024. 4

[58] Dongwei Pan, Long Zhuo, Jingtian Piao, Huiwen Luo, Wei Cheng, Yuxin Wang, Siming Fan, Shengqi Liu, Lei Yang, Bo Dai, Ziwei Liu, Chen Change Loy, Chen Qian, Wayne Wu, Dahua Lin, and Kwan-Yee Lin. Renderme-360: A large digital asset library and benchmarks towards high-fidelity head avatars. In *Advances in Neural Information Processing Systems 36: Annual Conference on Neural Information Processing Systems 2023, NeurIPS 2023, New Orleans, LA, USA, December 10 - 16, 2023*, 2023. 3

[59] Keunhong Park, Utkarsh Sinha, Jonathan T. Barron, Sofien Bouaziz, Dan B. Goldman, Steven M. Seitz, and Ricardo Martin-Brualla. Nerfies: Deformable neural radiance fields. In *2021 IEEE/CVF International Conference on Computer Vision, ICCV 2021, Montreal, QC, Canada, October 10-17, 2021*, pages 5845–5854. IEEE, 2021. 2

[60] Keunhong Park, Utkarsh Sinha, Peter Hedman, Jonathan T. Barron, Sofien Bouaziz, Dan B. Goldman, Ricardo Martin-Brualla, and Steven M. Seitz. Hypernerf: a higher-dimensional representation for topologically varying neural radiance fields. *ACM Trans. Graph.*, 40(6):238:1–238:12, 2021. 2

[61] Pascal Paysan, Reinhard Knothe, Brian Amberg, Sami Romdhani, and Thomas Vetter. A 3d face model for pose and illumination invariant face recognition. In *Sixth IEEE International Conference on Advanced Video and Signal Based Surveillance, AVSS 2009, 2-4 September 2009, Genova, Italy*, pages 296–301. IEEE Computer Society, 2009. 2

[62] William Peebles, Jun-Yan Zhu, Richard Zhang, Antonio Torralba, Alexei A Efros, and Eli Shechtman. Gan-supervised dense visual alignment. In *Proceedings of the IEEE/CVF Conference on Computer Vision and Pattern Recognition*, pages 13470–13481, 2022. 6

[63] Shenhan Qian, Tobias Kirschstein, Liam Schoneveld, Davide Davoli, Simon Giebenhain, and Matthias Nießner. Gaussianavatars: Photorealistic head avatars with rigged 3d gaussians. In *IEEE/CVF Conference on Computer Vision and Pattern Recognition, CVPR 2024, Seattle, WA, USA, June 16-22, 2024*, pages 20299–20309. IEEE, 2024. 2

[64] René Ranftl, Alexey Bochkovskiy, and Vladlen Koltun. Vision transformers for dense prediction. In *2021 IEEE/CVF International Conference on Computer Vision, ICCV 2021, Montreal, QC, Canada, October 10-17, 2021*, pages 12159–12168. IEEE, 2021. 4

[65] Daniel Roich, Ron Mokady, Amit H. Bermano, and Daniel Cohen-Or. Pivotal tuning for latent-based editing of real images. *ACM Trans. Graph.*, 42(1):6:1–6:13, 2023. 2, 3

[66] Shunsuke Saito, Gabriel Schwartz, Tomas Simon, Junxuan Li, and Giljoo Nam. Relightable gaussian codec avatars. In *IEEE/CVF Conference on Computer Vision and Pattern Recognition, CVPR 2024, Seattle, WA, USA, June 16-22, 2024*, pages 130–141. IEEE, 2024. 2

[67] Arman Savran, Nese Alyüz, Hamdi Dibeklioglu, Oya Çeliktutan, Berk Gökberk, Bülent Sankur, and Lale Akarun. Bosphorus database for 3d face analysis. In *Biometrics and Identity Management, First European Workshop, BIOID 2008, Roskilde, Denmark, May 7-9, 2008. Revised Selected Papers*, pages 47–56. Springer, 2008. 3

[68] Yichun Shi, Divyansh Aggarwal, and Anil K. Jain. Lifting 2d stylegan for 3d-aware face generation. In *IEEE Conference on Computer Vision and Pattern Recognition, CVPR 2021, virtual, June 19-25, 2021*, pages 6258–6266. Computer Vision Foundation / IEEE, 2021. 3

[69] Jingxiang Sun, Xuan Wang, Yichun Shi, Lizhen Wang, Jue Wang, and Yebin Liu. IDE-3D: interactive disentangled editing for high-resolution 3d-aware portrait synthesis. *ACM Trans. Graph.*, 41(6):270:1–270:10, 2022. 3

[70] Jingxiang Sun, Xuan Wang, Lizhen Wang, Xiaoyu Li, Yong Zhang, Hongwen Zhang, and Yebin Liu. Next3d: Generative neural texture rasterization for 3d-aware head avatars. In *IEEE/CVF Conference on Computer Vision and Pattern Recognition, CVPR 2023, Vancouver, BC, Canada, June 17-24, 2023*, pages 20991–21002. IEEE, 2023. 3

[71] Attila Szabó, Givi Meishvili, and Paolo Favaro. Unsupervised generative 3d shape learning from natural images. *CoRR*, abs/1910.00287, 2019. 3

[72] Jiaxiang Tang, Zhaoxi Chen, Xiaokang Chen, Tengfei Wang, Gang Zeng, and Ziwei Liu. LGM: large multi-view gaussian model for high-resolution 3d content creation. In *Computer Vision - ECCV 2024 - 18th European Conference, Milan, Italy, September 29-October 4, 2024, Proceedings, Part IV*, pages 1–18. Springer, 2024. 3

[73] Edgar Tretschk, Ayush Tewari, Vladislav Golyanik, Michael Zollhöfer, Christoph Lassner, and Christian Theobalt. Non-rigid neural radiance fields: Reconstruction and novel view synthesis of a dynamic scene from monocular video. In *2021 IEEE/CVF International Conference on Computer Vision, ICCV 2021, Montreal, QC, Canada, October 10-17, 2021*, pages 12939–12950. IEEE, 2021. 2

[74] Alex Trevithick, Matthew A. Chan, Michael Stengel, Eric R. Chan, Chao Liu, Zhiding Yu, Samih Khamis, Mammoohan Chandraker, Ravi Ramamoorthi, and Koki Nagano. Real-time radiance fields for single-image portrait view synthesis. *ACM Trans. Graph.*, 42(4):135:1–135:15, 2023. 3

[75] Ashish Vaswani, Noam Shazeer, Niki Parmar, Jakob Uszkoreit, Llion Jones, Aidan N Gomez, Łukasz Kaiser, and Illia Polosukhin. Attention is all you need. *Advances in neural information processing systems*, 30, 2017. 5

[76] Lizhen Wang, Zhiyuan Chen, Tao Yu, Chenguang Ma, Liang Li, and Yebin Liu. Faceverse: a fine-grained and detail-controllable 3d face morphable model from a hybrid dataset. In *IEEE/CVF Conference on Computer Vision and Pattern Recognition, CVPR 2022, New Orleans, LA, USA, June 18-24, 2022*, pages 20301–20310. IEEE, 2022. 3

[77] Tengfei Wang, Bo Zhang, Ting Zhang, Shuyang Gu, Jianmin Bao, Tadas Baltrusaitis, Jingjing Shen, Dong Chen, Fang Wen, Qifeng Chen, and Baining Guo. RODIN: A generative model for sculpting 3d digital avatars using diffusion. In *IEEE/CVF Conference on Computer Vision and Pattern Recognition, CVPR 2023, Vancouver, BC, Canada, June 17-24, 2023*, pages 4563–4573. IEEE, 2023. 2, 3

[78] Erroll Wood, Tadas Baltrusaitis, Charlie Hewitt, Sebastian Dziadzio, Thomas J Cashman, and Jamie Shotton. Fake it till you make it: face analysis in the wild using synthetic data alone. In *Proceedings of the IEEE/CVF international conference on computer vision*, pages 3681–3691, 2021. 6

[79] Yiqian Wu, Jing Zhang, Hongbo Fu, and Xiaogang Jin. LPFF: A portrait dataset for face generators across large poses. In *IEEE/CVF International Conference on Computer Vision, ICCV 2023, Paris, France, October 1-6, 2023*, pages 20270–20280. IEEE, 2023. 16

[80] Yuelang Xu, Bengwang Chen, Zhe Li, Hongwen Zhang, Lizhen Wang, Zerong Zheng, and Yebin Liu. Gaussian head avatar: Ultra high-fidelity head avatar via dynamic gaussians.

In *IEEE/CVF Conference on Computer Vision and Pattern Recognition, CVPR 2024, Seattle, WA, USA, June 16-22, 2024*, pages 1931–1941. IEEE, 2024. 2

[81] Lijun Yin, Xiaozhou Wei, Yi Sun, Jun Wang, and Matthew J. Rosato. A 3d facial expression database for facial behavior research. In *Seventh IEEE International Conference on Automatic Face and Gesture Recognition (FGR 2006), 10-12 April 2006, Southampton, UK*, pages 211–216. IEEE Computer Society, 2006. 3

[82] Lequan Yu, Xianzhi Li, Chi-Wing Fu, Daniel Cohen-Or, and Pheng-Ann Heng. Pu-net: Point cloud upsampling network. In *2018 IEEE Conference on Computer Vision and Pattern Recognition, CVPR 2018, Salt Lake City, UT, USA, June 18-22, 2018*, pages 2790–2799. Computer Vision Foundation / IEEE Computer Society, 2018. 5

[83] Wangbo Yu, Yanbo Fan, Yong Zhang, Xuan Wang, Fei Yin, Yunpeng Bai, Yan-Pei Cao, Ying Shan, Yang Wu, Zhongqian Sun, and Baoyuan Wu. NOFA: nerf-based one-shot facial avatar reconstruction. In *ACM SIGGRAPH 2023 Conference Proceedings, SIGGRAPH 2023, Los Angeles, CA, USA, August 6-10, 2023*, pages 85:1–85:12. ACM, 2023. 2

[84] Ziyang Yuan, Yiming Zhu, Yu Li, Hongyu Liu, and Chun Yuan. Make encoder great again in 3d GAN inversion through geometry and occlusion-aware encoding. In *IEEE/CVF International Conference on Computer Vision, ICCV 2023, Paris, France, October 1-6, 2023*, pages 2437–2447. IEEE, 2023. 3

[85] Mihai Zanfir, Thiendo Alldieck, and Cristian Sminchisescu. Phomoh: Implicit photorealistic 3d models of human heads. In *International Conference on 3D Vision, 3DV 2024, Davos, Switzerland, March 18-21, 2024*, pages 1229–1239. IEEE, 2024. 2

[86] Bowen Zhang, Yiji Cheng, Chunyu Wang, Ting Zhang, Jiaolong Yang, Yansong Tang, Feng Zhao, Dong Chen, and Baineng Guo. Rodinhd: High-fidelity 3d avatar generation with diffusion models. In *Computer Vision - ECCV 2024 - 18th European Conference, Milan, Italy, September 29-October 4, 2024, Proceedings, Part XIV*, pages 465–483. Springer, 2024. 2, 3

[87] Xing Zhang, Lijun Yin, Jeffrey F. Cohn, Shaun J. Canavan, Michael Reale, Andy Horowitz, Peng Liu, and Jeffrey M. Girard. Bp4d-spontaneous: a high-resolution spontaneous 3d dynamic facial expression database. *Image Vis. Comput.*, 32(10):692–706, 2014. 3

[88] Xing Zhang, Lijun Yin, Jeffrey F. Cohn, Shaun J. Canavan, Michael Reale, Andy Horowitz, Peng Liu, and Jeffrey M. Girard. Bp4d-spontaneous: a high-resolution spontaneous 3d dynamic facial expression database. *Image Vis. Comput.*, 32(10):692–706, 2014. 3

[89] Zicheng Zhang, Ruobing Zheng, Bonan Li, Congying Han, Tianqi Li, Meng Wang, Tiande Guo, Jingdong Chen, Ziwen Liu, and Ming Yang. Learning dynamic tetrahedra for high-quality talking head synthesis. In *IEEE/CVF Conference on Computer Vision and Pattern Recognition, CVPR 2024, Seattle, WA, USA, June 16-22, 2024*, pages 5209–5219. IEEE, 2024. 2

[90] Xiaochen Zhao, Lizhen Wang, Jingxiang Sun, Hongwen Zhang, Jinli Suo, and Yebin Liu. Havat: High-fidelity head avatar via facial model conditioned neural radiance field. *ACM Trans. Graph.*, 43(1):6:1–6:16, 2024. 2

[91] Mingwu Zheng, Hongyu Yang, Di Huang, and Liming Chen. Imface: A nonlinear 3d morphable face model with implicit neural representations. In *IEEE/CVF Conference on Computer Vision and Pattern Recognition, CVPR 2022, New Orleans, LA, USA, June 18-24, 2022*, pages 20311–20320. IEEE, 2022. 2

[92] Mingwu Zheng, Haiyu Zhang, Hongyu Yang, Liming Chen, and Di Huang. Imface++: A sophisticated nonlinear 3d morphable face model with implicit neural representations. *IEEE Trans. Pattern Anal. Mach. Intell.*, 47(2):994–1012, 2025. 2

[93] Yufeng Zheng, Wang Yifan, Gordon Wetzstein, Michael J. Black, and Otmar Hilliges. Pointavatar: Deformable point-based head avatars from videos. In *IEEE/CVF Conference on Computer Vision and Pattern Recognition, CVPR 2023, Vancouver, BC, Canada, June 17-24, 2023*, pages 21057–21067. IEEE, 2023. 2

[94] Hao Zhu, Haotian Yang, Longwei Guo, Yidi Zhang, Yanru Wang, Mingkai Huang, Menghua Wu, Qiu Shen, Ruigang Yang, and Xun Cao. Facescape: 3d facial dataset and benchmark for single-view 3d face reconstruction. *IEEE Trans. Pattern Anal. Mach. Intell.*, 45(12):14528–14545, 2023. 3

[95] Wojciech Zienolka, Timo Bolkart, and Justus Thies. Instant volumetric head avatars. In *IEEE/CVF Conference on Computer Vision and Pattern Recognition, CVPR 2023, Vancouver, BC, Canada, June 17-24, 2023*, pages 4574–4584. IEEE, 2023. 2

[96] Zi-Xin Zou, Zhipeng Yu, Yuan-Chen Guo, Yangguang Li, Ding Liang, Yan-Pei Cao, and Song-Hai Zhang. Triplane meets gaussian splatting: Fast and generalizable single-view 3d reconstruction with transformers. In *IEEE/CVF Conference on Computer Vision and Pattern Recognition, CVPR 2024, Seattle, WA, USA, June 16-22, 2024*, pages 10324–10335. IEEE, 2024. 5, 8

A. Appendix Overview

In this supplement, we present more visualization results in Sec. B, introduce our dataset generation and labeling process in Sec. C, discuss limitations of our work in Sec. D, and discuss ethical impacts in Sec. E.

B. More Visualization Results

In this section, we show more results of our framework as well as more comparisons with previous work.

360° synthesis results from our framework In Fig. 11, we render 360° images from our reconstructed Gaussian full-head given unposed images as input. As shown in the figure, after training on the proposed large-scale dataset, our framework can reconstruct Gaussian full-head and synthesize consistent novel view images.

More comparison results with previous methods on the testsets. In Fig. 12, we show more results of different methods on the testset. Four views of images are rendered from the reconstructed 3D representation of different methods, showing the full-head quality. As is shown in the figure, our framework gets much higher fidelity results and has fewer artifacts in unseen regions compared to previous works.

More comparison results with previous methods on real-world images. In Fig. 13, we show more results of different methods on real-world images sampled from the VFHQ dataset. As is shown in the figure, though trained on our synthesis only large-scale dataset, PanoLAM is able to generalize to the real-world images. Compared with previous methods, our framework reconstructs more texture details and maintains better identity fidelity.

C. Generation and labeling process for our large-scale synthesis dataset.

In this section, we introduce our dataset generation process and labeling strategy.

Dataset generation from trained 3D GANs. Given that EG3D is limited to rendering near-frontal images using its generated triplane NeRF, we sample images within a view range of approximately 72° from this model. Specifically, cameras are sampled from a pitch range of $\pm 26^\circ$ degrees and a yaw range of $\pm 36^\circ$ degrees relative to the front of the human face. To enhance the network’s adaptability to real-world images captured by various cameras, we vary the camera radius and focal length. The camera radius is drawn from a normal distribution centered at 2.7 with a standard deviation of 0.1, while the focal length is sampled from a

normal distribution centered at 18.83 with a standard deviation of 1. Each triplane generates 32 random images. For SphereHead [43], we generate 360° dataset. Specifically, we initially sample 8 views evenly spaced along the equatorial plane to ensure full-head coverage, dividing the 360-degree range. Additionally, we sample 24 images at random angles and apply the same randomization of camera radius and focal length as used in the EG3D sampling process. Visualization of some cases is shown in Fig. 14.

Dataset Labeling. Since the sampled data from 3D GANs may contain bad cases, which may hurt the training of the learning-based network. We also develop a labeling tool and remove bad cases manually to improve the dataset quality. Some examples of bad cases we removed are shown in Fig. 15.

D. Limitations

Our dataset and model are built upon 3D GANs trained on different 2D datasets, e.g., FFHQ [34] for EG3D and the WildHead [43], CelebA [50], FFHQ, LPFF [79], and K-Hairstyle [38] datasets for SphereHead. The proposed dataset is sampled from these trained 3D GANs, and the network trained on it has similar biases to these datasets. The sampled datasets contain less Asian data and no cartoon heads, leading to worse reconstruction results on Asian faces and bad results on cartoon faces from the proposed framework. A possible solution to this problem is to train the 3D GANs on a more diverse 2D dataset for more diverse 3D head avatar sampling and 3D avatar reconstruction network training. Our model only handles static full-head reconstruction, and the generated head is not animatable. We leave this as future work.

E. Ethical Impact

The generation of realistic avatars from images raises important ethical considerations, especially concerning privacy, consent, and the risks associated with the misuse of technology, such as the creation of deep fakes. It is essential to prioritize responsible use, ensuring adherence to ethical guidelines and standards to mitigate potential negative impacts.

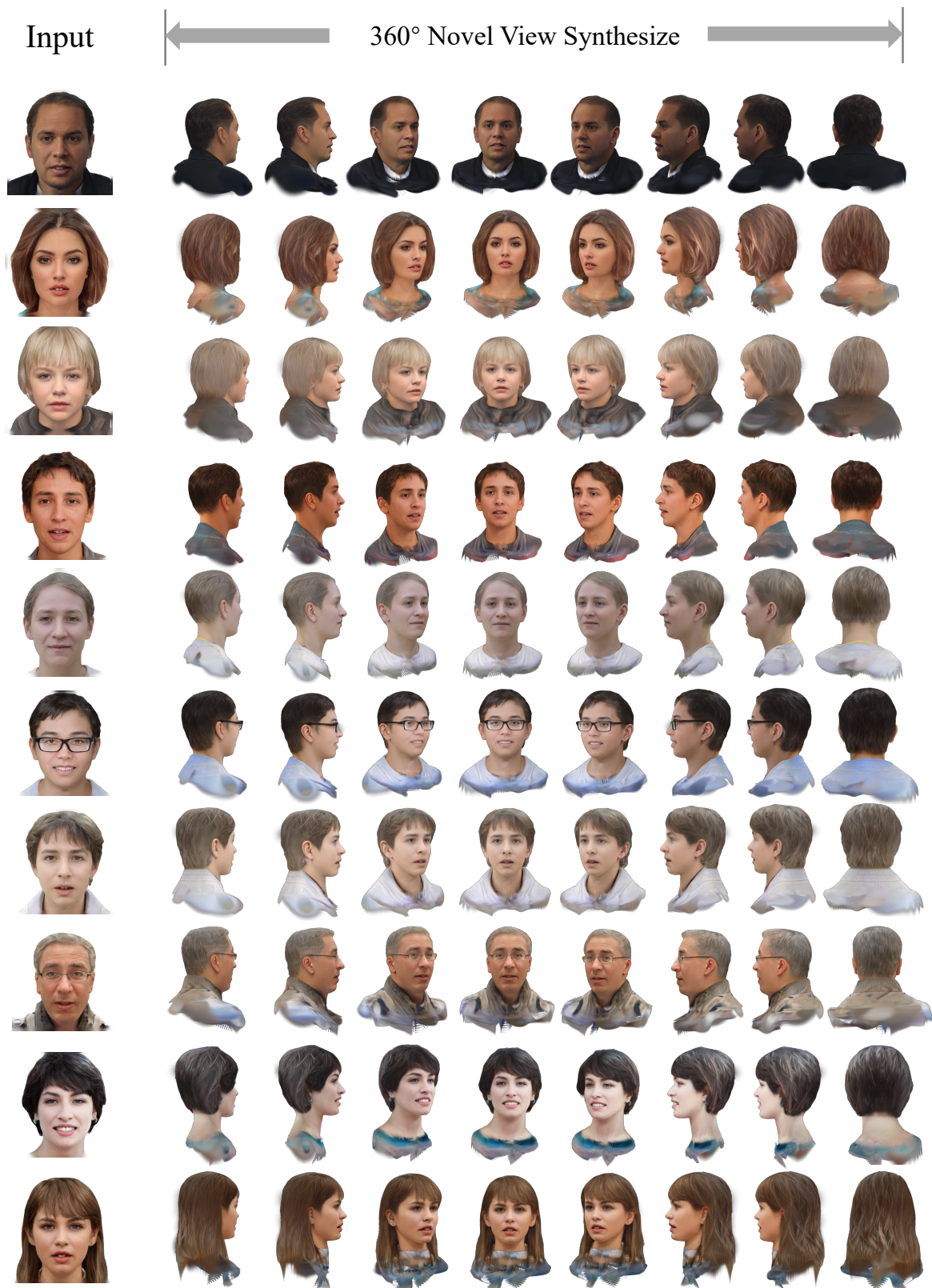


Figure 11. Visualization of our Gaussian full-head synthesis from one-shot unposed image.



Figure 12. Comparison of reconstruction and novel view synthesis of different methods on the testset.

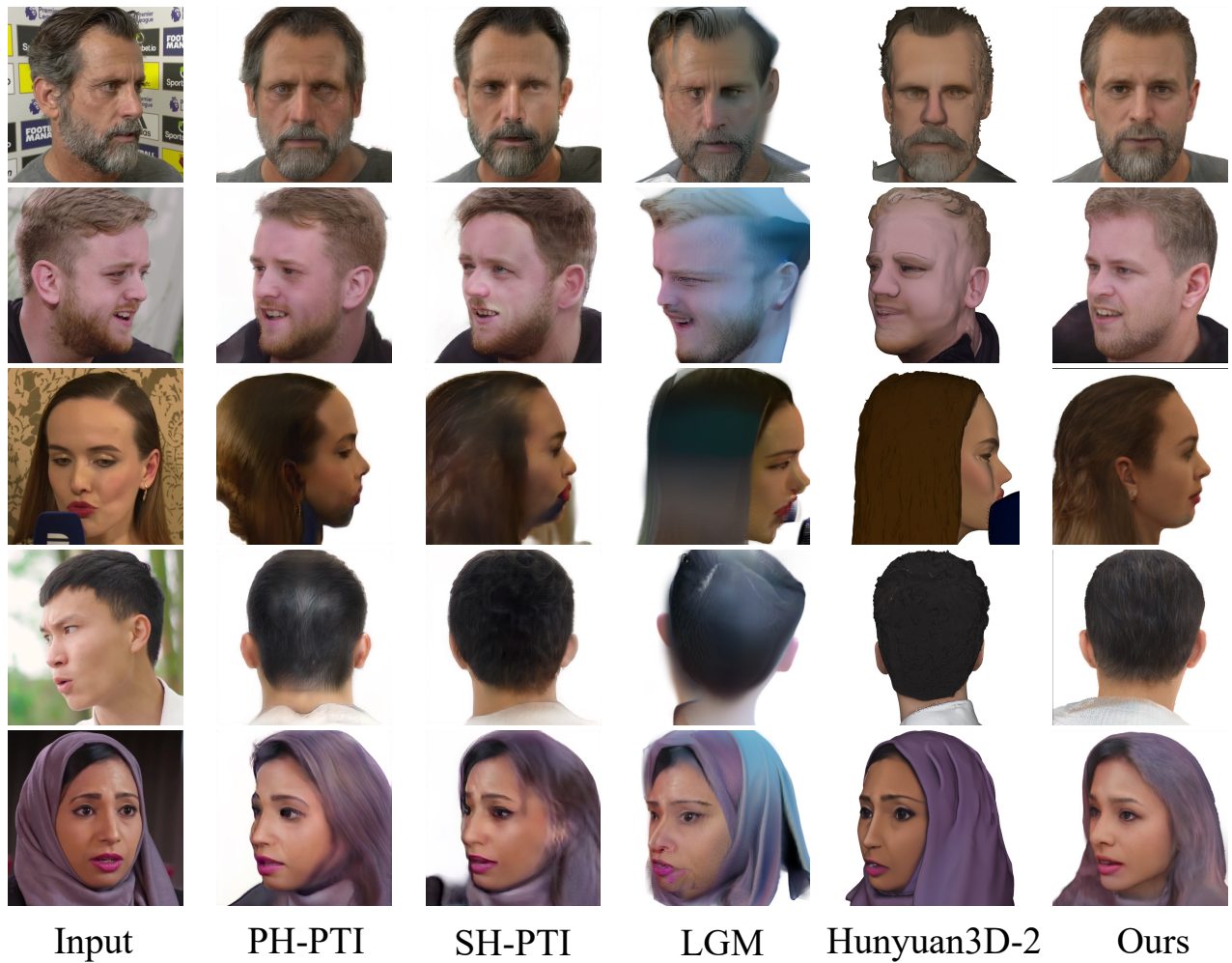


Figure 13. Comparison of reconstruction and novel view synthesis of different methods on in-the-wild real-world images.



Ours-Front from EG3D



Ours-360 from SphereHead

Figure 14. Visualization of example cases in our sampled and cleaned datasets.

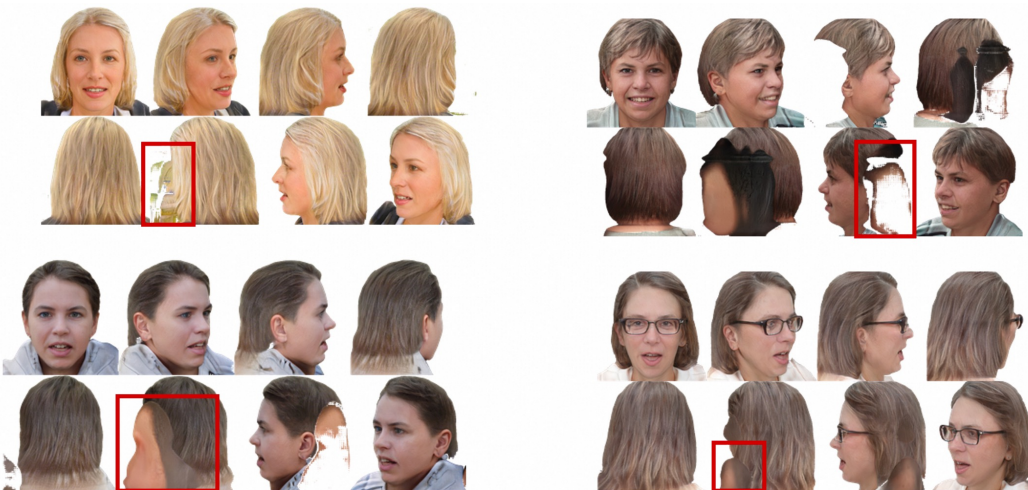


Figure 15. Examples of bad cases sampled from the 3D GANs prior, which are removed manually using our labeling tools.